Vertical distribution of aerosols over the Maritime Continent during El Nino

Jason Blake Cohen[1], Daniel Hui Loong Ng[2], Alan Wei Lun Lim[3], Xin Rong Chua[4]

[1]School of Atmospheric Sciences, Sun Yat-Sen University, Guangzhou, China
[2]Tropical Marine Science Institute, National University of Singapore, Singapore
[3]The Chinese University of Hong Kong, Hong Kong, China
[4]Princeton University, Princeton, NJ, USA

Correspondence to: Jason Blake Cohen (jasonbc@alum.mit.edu)

Abstract. The vertical distribution of aerosols over Southeast Asia, a critical factor of aerosol lifetime, and impact on radiative forcing and precipitation, is examined for the 2006 post El-Nino fire burning season. Additionally, through analysis of measurements and modeling, we have reconfirmed the hypothesis that fire radiative power is underestimated. Our results are significantly different from what others are using. The horizontally constrained Maritime Continent's fire plume median height, using the maximum variance of satellite observed Aerosol Optical Depth as the spatial and temporal constraint, is found to be 2.17 ± 1.53km during the 2006 El Nino season. This is 0.96km higher than random sampling and all other past studies, with 62% of particles in the free troposphere. The impact is that the aerosol lifetime will be considerably longer, and that the aerosols will disperse in a direction different from if they were in the boundary layer. Application of a simple plume rise model using measurements of fire properties underestimates the median plume height by 0.34km and more in the bottom-half of the plume. The center of the plume can be reproduced when fire radiative power is increased by 20% (range from 0% to 100%). However, to reduce the biases found, improvements are required in terms of measurements of fire properties when cloud covered, representation of small scale convection, and inclusion of aerosol direct and semi-direct effects. The results provide the unique aerosol signature of fire under El-Nino conditions.

1. Introduction

Properly quantifying the vertical distribution of aerosols is essential to constrain their atmospheric distribution, and in turn, the atmospheric energy budget [*Ming et al.*, 2010; *Kim et al.*, 2008], and understand their impact on circulation, clouds and precipitation [*Tao et al.*, 2012; *Wang* 2013], and human health [*Burnett et al*, 2014]. However, there are complicating factors including spatial and temporal heterogeneity in emissions [*Cohen and Wang*, 2014; *Cohen*, 2014; *Giglio et al.*, 2006; *Petrenko et al.*, 2012; *Wooster et al.*, 2012], and uncertainties and non-linearities associated with aerosol processing and removal from the atmosphere [Tao et al., 2012; *Cohen* and *Prinn*, 2011; *Cohen et al.*, 2011]. Furthermore, a lack of sufficiently dense measurements leads to difficulty constraining the measured distribution of aerosols over scales from hundreds to thousands of kilometers or over time frames on the decadal to longer time scales [Cohen and Wang, 2014; *Delene* and *Ogren*, 2002; *Dubovik et al.*, 2000; *Cohen* et al., 2017].

Models are very poor at reproducing the actual vertical distribution of atmospheric aerosols [*Cheng et al.*, 2012; *Schuster et al.*, 2005; *Tsigaridis et al.*, 2014]. They also tend to strongly underestimate the total atmospheric column loading of aerosols [*Colarco et al.*, 2004; *Leung et al.*, 2007]. Furthermore, vertical measurements are sparse, and in many regions do not provide adequate statistics to make informed comparisons with real world conditions. This is no more apparent than over Southeast Asia, where model studies [*Tosca et al.*, 2011; *Martin et al.*, 2012] have concluded that almost all aerosols are narrowly confined in the planetary boundary layer, although measurements demonstrate otherwise [*Lin et al.*, 2014]. Presently, there are no known modeling efforts that have been able to reproduce this significant atmospheric loading and the ensuing vertical distribution.

Additionally, aerosol emissions databases in Southeast Asia are quantified using a bottom-up approach, where small samples and statistics of the activity, land-use, economics, population, and hotspots are aggregated [*van der Werf*, 2010; *Lamarque*, 2010; *Bond et al.*, 2004]. This generally leads to sizable bias, since there are few measurements and rapidly changing land-surface features over Southeast Asia. A recent couple of papers, using measurements and models in tandem, has quantified a significant underestimation in aerosol emissions over Southeast Asia in terms of magnitude [*Cohen and Wang*, 2014], spatial, and temporal distribution [*Cohen*, 2014], including interannual and intraannual variation from fires.

Furthermore, the vertical distribution is uncertain due to incomplete understanding of in-situ production and removal mechanisms, which are dependent on washout, which is also poorly modeled [*Tao et al.*, 2012; *Wang* 2013], especially in the tropics during the dry season [*Petersen and Rutledge*, 2001; *Ekman et al.*, 2012], due to the random nature of convective precipitation. Heterogeneous aerosol processing may also change the hygroscopicity and hence vertical distribution of the aerosols [*Kim et al.*, 2008; *Cohen et al.*, 2011]. These factors have been show to combine such that small changes in the initial vertical distribution can lead to ultimate transport thousands of kilometers apart [*Wang,* 2013].

The Maritime Continent of Southeast Asia has faced widespread and ubiquitous fires the past few decades, due to expanding agriculture, urban development, economic growth, and changes in the base climatology that induce drought [*Center*, 2005; *Dennis et al.*, 2005; *van der Werf et al.*, 2008; *Taylor*,

2010]. These fires contribute the major fraction of the atmospheric aerosol burden during the dry season [*Cohen*, 2014]. However, these fires are unique: they are relatively low in radiative power and temperature, yet cover a massive net surface area, making their statistics and extent hard to characterize from remote sensing. Yet, their total emissions are very high and they dominate the aerosol optical depth (AOD) and $PM_{2.5}$ levels over thousands of kilometers [*Field et al.*, 2009; *Nakajima et al.*, 1999]. Due to their widespread nature, fires in this region are geospatially coherent in their timing and geography, although individually they burn for different lengths of time, as a function of localized precipitation and soil moisture, and global circulation patterns such as El-Nino [*Cohen*, 2014; *Wooster et al.*, 2012; *Hansen*, 2008].

A comprehensive previous attempt to study aerosol height over Southeast Asia was performed by Lee et al. [2016]. They used the total CALIOP profile, but were not specific about how they cleared or accounted for high ice clouds that frequently found in this part of the world. Furthermore, they used satellite derived SSA to provide additional spatial resolution to go with each pass, but which has been shown to be highly error-prone over Southeast Asia [Rogers et al., 2009; Hostetler, 2008]. This work did not address how the spatially-disparate individual path measurements from CALIOP, sampling both fire plume and non fire plume pixels jointly, as compared to the approach used by Cohen [2014] and Cohen et al. [2017]. The few other attempts using CALIOP over this region have also been done, but without any local validation of the CALIOP product [Sugimoto et al., 2015], or have used models to validate the CALIOP measurements [Campbell et al., 2013].

This work describes a new approach to comprehensively sample the vertical distribution of smoke aerosols, by first using decadal scale measurements of AOD from the MISR satellite [*Cohen*, 2014], and then separating the smoke impacted regions by the magnitude of the measured variability. During the 2006 El-Nino enhanced burning, one of the 2 largest such events over the past 15-year measurement record, this approach yields a much higher vertical aerosol height than the traditional random sampling approach. A simple plume-rise model [*Achtemeier et al.*, 2011; *Briggs*, 1965] using reanalysis meteorology [*Kalnay et al.*, 1996] and measured fire properties was found to underestimate the measured heights. However, the model could be improved to match the median heights by increasing the measured fire radiative power [*Sessions et al.*, 2011; *Sofiev et al.*, 2012], implying that the measured fires may be underestimated in terms of their strength, or that there are missing fires. However, the top and bottom heights of the measured plume still cannot be reproduced. The data shows that an improved representation of both localized convective transport and the aerosol direct and semi-direct effects [*Ekman et al.*, 2007; *Wang*, 2007] are required to make further improvements. It is hoped that these results will provide insight to those working on understanding the strong 2015-2016 El-Nino conditions.

2. Methods

2.1 Geography

This work is focused on the Maritime Continent, a sub region of Southeast Asia (8^oS to 8^oN, 95^oE to 125^oE) (**Figure 1**) that experiences wide-spread and highly emitting fires on a yearly basis during the

local dry season (August to October/November). The combined magnitude of the fires produces a single massive smoke plume, that covers much of the region, extending thousands of kilometers [*Cohen*, 2014]. These wide spread fires are due to anthropogenic clearing of rainforest and agriculture [*Cohen* et al., 2017; *Dennis et al.*, 2005; *van der Werf et al.*, 2008; *Taylor*, 2010; *Miettinen et al.*, 2013; *Langmann et al.*, 2009]. Over this region, during the dry season, the removal of aerosols is quite slow, leading to the overall properties of the plume being relatively consistent over space and time [*Cohen*, 2014]. Therefore, the overall properties of the smoke plume, when correctly bounded in space and time, can be robustly statistically related to the overall properties of individual fires, and daily measurements of AOD from the MISR satellite (**Figure 1**) [*Cohen*, 2014].

In 2006, the El-Nino conditions led to an enhanced drought, with subsequent fires lasting from September through November. To ensure that this event is uniquely and completely analyzed, only data from October is used. The region in (**Figure 1**) with the EOF (Bjornsson and Venegas, 1997; Cohen et al., 2017) of the measured MISR AOD larger than 2.2 is the net of the source regions (over land) and downwind regions (over both land and sea). This analytically provides a holistic representation in space and time of the impact of individual fires on the large-scale structure of the aerosol plume, hence allowing a comprehensive sampling of the vertical distribution of the smoke, including all sources, both observed and obscured by clouds (very common in this region), and aged aerosols downwind from their initial sources.

2.2 Measurements

CALIPSO is an active lidar that quantifies both the vertically resolved atmospheric backscatter strength (a reasonable approximation of the vertical profile of aerosols), and an indication of particle size (large or small) [*Winker et al.*, 2003]. Specifically, we use the backscatter at 532nm and the vertical feature mask (vertical resolution 30m, horizontal resolution 1/3km) [*Hostetler et al.*, 2006]. Since the width of each pass is narrow, they are not spatially representative in general. However, given the relative consistency of the plume as a whole, samples constrained within the plume's spatial extent, taken on the same day, are statistically representative of the smoke plume as a whole [*Cohen*, 2014].

The extinction-weighted top (10% vertically integrated height), middle-upper (30% vertically integrated height), median (50% vertically integrated height), middle-lower (70% vertically integrated height), and bottom (90% vertically integrated height) are computed for each individual measurement, with the values retained if the aerosol is not in the stratosphere (assumed to be 15km) (**Supplemental Figure 1**). The data is then aggregated first by day, and secondly by geography, either into the fire-impacted region, or non fire-impacted region, based on (**Figure 1**) [*Cohen*, 2014]. The aggregated set of measurements is used to compute probability densities and statistics, demonstrating the vast difference over the fire-impacted and non-fire impacted regions (**Figures 2a,2b)**. with the vertical heights both significantly higher and less variable ($p<0.01$) over the fire region than the non-fire region.

Measurements of aerosol optical depth (AOD) [*Kaufman et al.*, 2003], fire radiative power (FRP) and fire temperature (T_F) [*Freeborn et al.*, 2014; *Ichoku et al.*, 2008] are obtained from the MODIS instrument aboard both the TERRA and AQUA satellites. Version 5, level 2, swath-by-swath measurements,

at daily resolution are use for AOD (best solution 0.55 micron), with a spatial resolution of 10kmx10km, and FRP/T_F, with a spatial resolution of 1kmx1km. Given the prevalence of clouds in this region, the cloud-cleared products are used, leading to a possible low bias in the FRP/T_F measurements, as well as some fires not measured at all [*Cohen* et al., 2017; *Freeborn et al.*, 2014; *Ichoku et al.*, 2008; *Kahn et al.*, 2008; *Kahn et al.*, 2007]. On the other hand, while some grids are contaminated, the sheer spatial distance of the plume and the fact that the overwhelming majority of atmospheric aerosols during this time of the year are due to fires, means that there is no observable bias in the overall statistics of the measured AOD [*Cohen*, 2014], as observed by looking at the spatially averaged MODIS AOD and statistics over the fire-constrained and non fire-constrained regions (**Figure 3**). The AOD is higher ($p<0.01$) over the fire-constrained region, making the findings consistent with the approach employing the 12 years worth of MISR measurements.

In terms of MODIS retrieval uncertainties over land, especially during fire events, there are two important issues to consider. The first is that under extremely high AOD conditions (AOD>2), frequently aerosols are flagged/reclassified as clouds, which brings about a negative bias. This bias would lead to an even higher AOD over the fire plume region if it were properly handled, leading to an even larger difference between "fire region" and the "non-fire region". The second is the error in the over-land retrieval can go as high as 15%. However, based on the results in (**Figure 3 and Supplemental Figure 2**), the difference between the "fire region" and the "non-fire region" is statistically sound even assuming the error is larger than 15%. It is also the reason why MISR was used for the initial definition of the two regions, since its ability to cloud clear is better than MODIS over this region.

While there are are many errors involved with using the satellite data, the errors in this case are sufficiently small as to not impact the analysis and results over Southeast Asia during the fire season (Cohen, 2014; Cohen et al., 2017). The AOD and certain surface products, when used to run models, have been found to compare in magnitude, spatial, and temporal extent, to various ground based surface and column measurements, such as from AERONET, NOAA, and national pollution networks. The data-driven models have been shown to lead to a reduction in the annualized RMS error as compared with the IPCC RCP emissions scenarios by a factor of 2 to 8 against AERONET stations throughout Asia (Cohen and Wang, 2014). Furthermore, on a month-to-month basis, the results of the data-driven models have been shown to lead to a reduction in the RMS error by a factor of 1.8 and an improvement in the R2 statistic of 0.2 to 0.3 against the GDED Fire emissions dataset (Cohen 2014; Cohen et al. 2017). Given these findings, it is reasonable to assume that the methodology is as reliable as anything else presently available, with respect to this work.

2.3 Plume Rise Model

A simple model is employed to simulate the height to which a parcel of air initially at the surface over the fire will rise, based on buoyancy, vertical, and horizontal advection (**Supplement**). The formulation requires information about the temperature and radiative power of the fire as well as local meteorology [*Achtemeier et al.*, 2011; *Briggs*, 1965], and yields an idealized height to which aerosols

emitted will rise. The buoyant plume rise is a thermodynamic approximation in nature and thus not as physically realistic as a large eddy approach, which solves the atmospheric fluid dynamical equations by parameterizing turbulence at the scale of tens of meters. However, it is less computationally expensive and more generalizable in the context of approximating the thousands of fires spread geographically over hundreds of thousands of square kilometers. On the other hand, it is more physically realistic than empirical relationships from multi-angle measurements [*Sofiev et al.*, 2012], which have also been attempted, but show poor performance in Southeast Asia.

These relationships are efficiently solved using measurements of meteorological and fire properties, allowing them to be used as rapid parameterizations within regional or global models. However, there are errors associated with reconciling the different temporal and spatial scales of reanalysis meteorology, especially convection and associated transport. Secondly, cloud-cover in this region leads to both missing fires and low-bias in measurements of fire properties [Sofiev et al., 2012; *Kaufman et al.*, 2003]. Third, the cloud-cover also leads to a heavier contribution of model results in the reanalysis meteorology. Finally, the effects of the optically thick aerosol plume's feedback on the radiative profile is likely important, but beyond the scope of this work and hence not taken into consideration [*Ekman et al.*, 2007; *Wang*, 2007].

3. Results and Discussion

3.1 Measured Aerosol Vertical Distribution

The fire-constrained monthly aggregated daily statistics of the measured vertical aerosol height from CALIPSO [*Winker et al.*, 2003] is given in (**Figure 2a**), with the monthly aggregated statistics over the fire-constrained region of the bottom, middle-lower, median, middle-upper, and top heights respectively: 1.68 ± 1.59km, 1.92 ± 1.55km, 2.17 ± 1.53km, 2.50 ± 1.54km, and 2.98 ± 1.55km (**Table 1**). On the other hand, the non fire-constrained region's monthly aggregated statistics of the measured vertical aerosol height is quite different (**Figure 2b**), with the respective bottom, middle-lower, median, middle-upper, and top heights: 0.65 ± 0.98km, 0.93 ± 0.98km, 1.21 ± 1.00km, 1.53 ± 1.02km, and 1.98 ± 1.08km (**Table 1**). The average aerosol height over the fire-constrained region is both much higher and more variable at every vertical level as compared to the non fire-constrained domain, with 62% of the aerosol loading in the free troposphere over the fire-constrained domain, while only 17% is located in the free troposphere over the non fire-constrained domain. However, the variability is roughly constant at all levels over the fire-constrained region, while the variability increases with vertical level, over the non fire-constrained region. These results are based on more than 10,000 daily CALIOP measurements.

All three findings, higher average aerosol height, larger variance of height, and a consistent variance of height at all levels, are consistent with areas where most of the aerosol loading is due to surface fires. Firstly, the buoyancy from fires increases the expected height, with differences in buoyancy from different strength fires producing random variability in the measured heights. So long as the distribution of fire strength and meteorology do not differ too much from day-to-day, the variance in aerosol heights should also not vary much. On the other hand, over non fire-constrained regions, the major contribution to

213 the vertical aerosol variability is convection, which is expected to increase in variability the higher one
214 moves upwards from the surface.
215 Furthermore, the relatively constant variability across the heights in the fire-constrained region is
216 consistent with a proposed radiative-stabilization effect. The extremely high measured AOD values found
217 by MODIS [*Kaufman et al.*, 2003] over the fire-constrained domain (from 0.5 to 2.0, with most days over
218 1.0), leads to observable surface cooling (**Figure 3**). Additionally, BC emitted from the fire, absorbs
219 incoming solar radiation near the upper portion of the plume, providing a source of warming. This
220 combination leads to additional stabilization of the atmosphere, and therefore the vertical aerosol
221 distribution.
222 These results are thus consistent with the observed reduction in in-situ vertical processing over the
223 regions downwind from the fire sources, but still within the fire-constrained plume region, where buoyancy
224 from the fires and the self-stabilization effect seem to contribute more than random deep convection.
225 However, over the non fire-constrained region, given the low AOD and lack of fires, both of these effects
226 are not observed, and convection dominates, which is consistent with the less uniform vertical distribution.
227 Given these clear and observed differences, only results from the fire-constrained region will be considered
228 further.
229 A significant amount of aerosol mass exists in the free troposphere over this region. By assuming
230 that the measured boundary layer height of 1000m as observed in Singapore [*Chew et al.*, 2013] is applied
231 to the domain, then 62%, 73%, 83%, 93%, and 98% of the total monthly respective measurements of the
232 bottom, lower-middle, median, upper-middle and top extinction heights are located in the free troposphere.
233 This is much higher than previous studies, which indicated most of the smoke remained within the
234 boundary layer [*Tosca et al.*, 2011].
235 Analysis of the daily measured heights demonstrates 3 statistically unique days: October 11th, 15th
236 and 22nd (**Table 2**). On the 11th, the top and upper-middle measurements fall within the top 15%, while the
237 median measurements fall within the top 20% of the month's measurements, implying that the result is
238 consistent with a deep, single layer, extending throughout the lower and middle free-troposphere. The 15th
239 and 22nd, while not being as high in the middle-troposphere, also have little to no aerosol in the planetary
240 boundary layer due to being more confined in the vertical, implying a narrow layer in the middle free-
241 troposphere. These results are consistent with the measured aerosol layer being mostly in the free
242 troposphere, a result that is not consistent with the measured FRP or meteorology, leading to two important
243 implications. Firstly, the aerosol lifetime on these days will be considerably longer than models typically
244 reproduce and the radiative forcing will be considerably more warming. Secondly, that typical modeling
245 approach that fresh aerosols are mixed from the surface to the given top of the plume height is likely not
246 true here, which has implications for the ability of most models to be able to correctly capture the aerosol
247 loading.
248 On the remaining days, the measured heights are consistent on a daily average basis with relatively
249 uniform emissions, meteorology, and vertical buoyant rise. Although present, intense but heterogeneous

forcing impacting the vertical distribution, such as localized convection and aerosol cloud interactions are generally not observed to bias the overall plume's properties. Only on October 11th, 15th, and 22nd, are there higher heights or a narrower vertical structure, combined with no readily available explanation to be found in the fire, AOD, or meteorological properties on these days, indicating a likely clear change in the convection on those days, or some other phenomena not considered or captured by the reanalysis meteorology. The robustness of this approach assures the validity over the region and time period considered herein.

A comparison between the inverse model by Campbell et al. [2013; Supplemental Figure 6] and this work's underlying Kalman Filter plus variance maximization inversely modeled fields, shows that their model performs considerably less well during the biomass burning season, which is the focus of this work [Cohen, 2014; Cohen and Wang, 2014; Cohen et al., 2017]. Furthermore, the results found using the approach employed here, match well with individual measurement campaigns done by Lin Neng-Hui, et al. [2013, 2014, etc.], and the AD-Net measurement network [Sugimoto et al, 2014], that have focused on observations from a small number of on-the-ground lidar at multiple places within the Northern portion of Southeast Asia and Greater East Asia. While the geographic regions are not identical and therefore cannot be used to directly validate the region studied here, there is a sufficient amount of similarity, that there is some likelihood of overlap in the results. Given these factors, we present the results here as the best available for use at this time, when targeting this region of the world during the biomass burning season.

3.2 Measured Fire and Meteorological Properties

The daily aggregated measurements of fire radiative power (FRP) [*Freeborn et al.*, 2014; *Ichoku et al.*, 2008] indicate there are 109395 actively burning 1kmx1km pixels in October 2006. However, filtering for high confidence [Level 9] active fires, reduces this number to 6941 1kmx1km pixels. The respective measurements have 10%, median, and 90% values of FRP of [115,300,975] W/m^2 for all fires and [185,540,1495] W/m^2 for high confidence fires (**Table 3**). Overall, these values are much lower than FRP measured over other intensely burning regions [*Giglio et al.*, 2006]. However, the results are consistent with the fact that fires in the Maritime Continent occur under relatively wet surface conditions, due to high levels of mineral-soil moisture, extensive peat, and intermittent localized precipitation [*Couwenberg et al.*, 2010]. These results are based on more than 3000 daily MODIS fire hotspots and associated meteorological measurements.

There is only one day, October 2nd, with a statistically high FRP (daily mean more than monthly 90% value), for high confidence fires. Similarly, there are two days, October 28th and 30th, with an abnormally low FRP (daily mean less than monthly 15% value), for high confidence fires. None of these days have a statistically abnormal fire vertical height distribution. However, October 28th and 30th both show a sizable increase in AOD over the fire constrained region, with the AOD more than 2 standard deviations greater than the mean over the non fire constrained region, as compared to the period of time from the 25th through the 27th.One consistent rationale is that there was large-scale precipitation increasing aerosol removal and subsequently wetting the surface. This in turn led to lower temperature and FRP and

correspondingly higher aerosol emissions factor on these days. Overall, there is no apparent impact of day-to-day variability of measured FRP driving observed variation in measured aerosol heights, and hence only high confidence fire data is subsequently used.

MERRA [Rienecker et al., 2011] reanalysis meteorology is used for the horizontal and vertical wind, and vertical temperature profile at each location where a fire is measured (**Table 3**). MERRA was chosen because it is based on NASA satellite measurements, and thus should be more consistent with the measurements used here. With the exceptions of October 5th and 20th, the horizontal wind is relatively calm 6.0 ± 1.3m/s. Also, throughout the entire month, the vertical temperature gradient is relatively stable -5.45 ± 0.16K/km, with only 7 individual fires occurring under unstable atmospheric conditions. Therefore, dynamical instability is not expected to contribute greatly to the vertical distribution [*Stone and Carlson*, 1979]. Also, the role played by the large-scale vertical wind is small 2.1 ± 1.6mm/s. Given the atmospheric stability and fire-controlled buoyancy conditions, the plume rise model approach should offer a reasonable approximation of the aerosol vertical distribution.

The approach used here relies upon the atmosphere being either stable or only minority non-stable. However, in general in this part of the world, there are two reasons that would contribute to most fires occurring under such conditions: firstly, that major instability would frequently lead to rain, fire suppression, and aerosol wash-out; and secondly that the induced surface cooling and atmospheric heating by the extensive aerosol layer itself would tend to increase the atmospheric stability. Such points are made clear in terms of the major unaccounted for processes in the MERRA data at this resolution, being: localized convection (due to the resolution), and the aerosol cooling and in-situ heating effects (not incorporated into MERRA's underlying model). In theory the direct and semi-direct effect may be able to be parameterized, but this would require a higher order model. Hence, since these conditions and effects are not considered by the plume rise model, they therefore cannot be explanations for discrepancies in the modeled vertical distribution.

3.3 Modeled Aerosol Vertical Distribution

Applying the plume rise model, the aggregated daily statistics of the vertical aerosol height at the bottom, lower-middle, median, upper-middle, and top are 0.60km, 1.14km, 1.85km, 2.87km, and 4.99km respectively (**Figure 4, Table 4)**. The mean daily median, lower-middle, and bottom modeled heights are lower than the respective mean measured heights by 0.48km, 0.78km, and 1.07km respectively, with a wide underestimate day-to-day ranging from 1.91km to 1.11km. The upper-middle modeled height is about equal to measurements, with a mean difference of 0.03km, and wide day-to-day variations, from an overestimate of 1.97km to an underestimate of 1.36km. Finally, the top modeled heights are considerably higher than measurements, with an average overestimate of 1.02km, and a day-to-day range from an overestimate of 3.96km to an underestimate of 0.44km.

The model underestimates the height of the median through bottom of the plume, while simultaneously overestimating the top. First, this means that the model is not accounting for enough energy to obtain the average rise of the plume. At the same time, the modeled vertical spread is too large, implying

other factors limit the height gain near the top of the plume while simultaneously enhance the height near the bottom. The results are consistent with one or both of the two hypothesized effects; first, that a low bias exists in the measured values of FRP [*Kahn et al.*, 2007; *Kahn et al.*, 2008], leading to insufficient buoyancy; and second, that in-situ stabilization occurs due to aerosol radiative cooling in the lower parts of the plume and aerosol radiative heating within the upper parts of the plume. This combination of factors is also consistent with the observed underestimate in measured FRP to match the median height, as well as the hypothesized complete non-detection of small fires [*Kaufman et al.*, 2003]. There are also uncertainties in the MERRA reanalysis products, but given the large sample size and the narrowness of the MERRA distribution, the impact of these uncertainties is considerably smaller than changes in the FRP on the order of 10%.

A sensitivity analysis is used to quantify the effects of a low bias in FRP, by applying a constant multiplicative factor to the measured FRP for each fire, from 1.0 to 2.0 in steps of 0.1 (although only the results in steps of 0.2 are given in **Table 4**). Although there are also uncertainties associated with measured vertical wind and temperature structure, this is not considered (**Table 3**), since there is no way to couple meteorological effects at sub-grid scale, or otherwise not included in the reanalysis meteorology. The results are obtained by minimizing the root-mean square (RMS) difference between the daily measured and modeled heights, for each FRP scaling factor, at each of the middle-upper, median, and middle-lower levels. The respective best-fit enhancement factors are **1.0** for middle-upper measurements (RMS=0.94km), **1.2** for median measurements (RMS=0.81km), and **2.0** for middle-lower measurements (RMS=0.74km) (**Table 4**). Although there is no single best-fit FRP scaling factor, the results produce a better fit to measured values from the middle-lower to the middle-upper than using the model without any FRP enhancement.

The results establish that current plume rise models can reproduce the median vertical plume height over Southeast Asia by increasing the FRP by 20%, a finding consistent with FRP generally underestimated over this region. By changing the FRP enhancement from 0% to 100%, the central height of the plume can be modeled, although the top and bottom heights of the plume cannot be reproduced. Additionally, the modeled plume is widely spread as compared to the narrowness of the measured plume. Unfortunately, rectifying these limitations will likely require the use of a more complex modeling approach and improvement of measured fire data.

There are additional errors associated with the non-complete complexity of the models employed. The models do not capture the contribution of atmospheric stabilization due to both the direct and semi-direct aerosol effects. Furthermore, these models do not take into account the impacts of localized convection. However, the majority of other works that employ regional and global models use this exact same methodology, and hence they also neglect these same small-scale phenomena in terms of communication between the chemistry, radiation, and the meteorology.

4. Conclusions

This work comprehensively quantifies the significant present-day underestimation of the vertical distribution of aerosols over the Maritime Continent during an El-Nino influenced fire season, by introducing a new method to appropriately constrain the measurements over the geographical region of the aerosol plume. While this was a large-scale fire event, it was very special, because it occurred throughout the month of October, whereas typically the wet-season arrives sometime within the middle of the month. As such, the wetness of the soil and the large-scale meteorological flow, were both different this year from a more typical year. As a result, the measured heights over the constrained region are found to be higher than previously thought, with about 62% of aerosols found in the free troposphere, where they can be advected thousands of kilometers and have more impact on the atmospheric and climatic systems. Additionally, over the fire-constrained region, the vertical variability of the plume is found to be uniform throughout its height, implying that it is controlled mostly by local forcing, such as the buoyancy released by fires, localized convection, and aerosol/radiative feedbacks, such as the direct and semi-direct effects.

Application of a plume-rise model showed that there was an overall low bias against measured heights, which is consistent with the FRP being underestimated in this region of the world due to large-scale cloud cover. It was also determined that measured vertical heights are more narrowly confined than model simulations. Applying a robust sensitivity analysis found that the middle-lower through middle-upper extent of the plume can be reproduced if an appropriate (although changing) enhancement is applied to the FRP ranging from 1.0*FRP to 2.0*FRP (with 1.2*FRP the best fit-value). Hence, the variable FRP enhancement factor approach can allow for improved modeling of the height statistics for the middle-upper to middle-lower extent of the plume.

However, it is not possible to reproduce either the top or bottom of the measured heights, the knowledge of which is important to constrain the impacts of long-range transport and aerosol-climate interactions. Nor is it possible to reproduce the narrow spread of the measured heights. The results are consistent with the general understanding of current model shortcomings, which in addition to the underestimated FRP values, will also need to be addressed. Hence, the current community-wide dependence on FRP measurements for vertical aerosol modeling may lead to flaws in our being able to successfully model the distribution.

The results have been found to be robust over a region that behaves roughly uniformly over thousands of kilometers and includes regions both near and far from the source of the fires. Since there are only a few days that have relatively unique aerosol and meteorological properties over the period studied, the results support the most important aspect of improving the aerosol heights will be newer modelling approaches and improvements that will be able to resolve local-scale forcing, such as deep convection, aerosol/radiation interactions, and aerosol-cloud interactions. Secondly, the biased underestimation of FRP is also an important point to improve the aerosol height modeling, especially under conditions where cloudiness occurs or the measured AOD levels are very high. These errors are exacerbated over regions where large-scale precipitation is very low or where there is substantial aerosol/cloud intermixing. In all

cases, until these model and measurement improvements are made, there is expected to be a significant underestimation of the aerosol loadings and radiative forcing distribution regionally, and to some extent globally. It is hoped that in the interim, the community will adapt a variable enhancement of FRP in tandem with measurement-constrained boundaries of smoke plumes, as a way to more precisely reproduce the statistics of the vertical aerosol distribution.

Acknowledgements:

We would like to acknowledge the PIs of the NASA MODIS, MISR, and CALIPSO projects for providing the data. The work was supported by the Chinese National Young Thousand Talents Program (Project 74110-52601113), and the Chinese Ministry of Science and Technology (Project 74110-41110002).

405 **References:**

406 Achtemeier, G., S. Goodrick, Y. Liu, F. Garcia-Menendez, Y. Hu, and M. Odman, (2011). Modeling smoke
407 plume-rise and dispersion from Southern United States prescribed burns with daysmoke.
408 Atmosphere, 2, 358-388.

409 Bjornsson, H. and Venegas, S, (1997). A Manual for EOF and SVD Analyses of Climate Data. Department
410 of Atmospheric and Oceanic Sciences and Centre for Climate and Global Change Research, Tech.
411 rep., McGill University, Technical Report, 1997.

412 Bond, T. C., D.G. Streets, K.F. Yarber, S.M. Nelson, J.H. Woo, and Z. Klimont. (2004). A technology-based
413 global inventory of black and organic carbon emissions from combustion, J. Geophys. Res., 109,
414 D14203, doi:10.1029/2003JD003697.

415 Briggs, G. A. (1965). A plume rise model compared with observations. *Journal of the Air Pollution Control*
416 *Association*, vol. 15, no. 9, pp. 433–438.

417 Burnett, R., A. Pope, M. Ezzati, C. Olives, S. Lim, S. Mehta, H. Shin, G. Singh, B. Hubbell, M. Brauer, R.
418 Anderson, K. Smith, J. Balmes, N. Bruce, H. Kan, F. Laden, A. Pruss-Ustun, M. Turner, S. Gapstur,
419 R. Diver, and A. Cohen. (2014) An Integrated Risk Function for Estimating the Global Burden of
420 Disease Attributable to Ambient Fine Particulate Matter Exposure, Environ Health Perspect;
421 doi:10.1289/ehp.1307049.

422 Campbell, J.R., Reid, J.S., Westphal, D.L., Zhang, J.L., Tackett, J.L., Chew, B.N., Welton, E.J., Shimizu,
423 A., Sugimoto, N., Aoki, K., Winker, D.M. (2013) Characterizing the vertical profile of aerosol
424 particle extinction and linear depolarization over Southeast Asia and the Maritime Continent: The
425 2007–2009 view from CALIOP, Atmospheric Research, 122, March 2013, 520–543,
426 http://dx.doi.org/10.1016/j.atmosres.2012.05.007.

427 Chew, B. N., J.R. Campbell, S.V. Salinas, C.W. Chang, J.S. Reid, E.J. Welton, and S.C. Liew. (2013).
428 Aerosol particle vertical distributions and optical properties over Singapore. *Atmospheric*
429 *Environment*, *79*, 599-613.

430 Chung, C. E., V. Ramanathan and D. Decremer. (2012) Observationally constrained estimates of
431 carbonaceous aerosol radiative forcing, *Proc. Natl. Acad. Sci. U.S.A.*,
432 doi:10.1073/pnas.1203707109.

433 Cohen, J. B. and Prinn, R. G. (2011). Development of a fast, urban chemistry metamodel for inclusion in
434 global models, Atmos. Chem. Phys., 11, 7629–7656, doi:10.5194/acp-11-7629-2011.

435 Cohen, J. B. (2014) Quantifying the occurrence and magnitude of the Southeast Asian fire climatology.
436 *Environmental Research Letters*, *9*(11), 114018.

437 Cohen, J. B., Lecoeur, E., and Hui Loong Ng, D. (2017) Decadal-scale relationship between measurements
438 of aerosols, land-use change, and fire over Southeast Asia, Atmos. Chem. Phys., 17, 721-743,
439 doi:10.5194/acp-17-721-2017.

440 Cohen, J. B. and Wang C (2014) Estimating Global Black Carbon Emissions Using a Top-Down Kalman
441 Filter Approach. *J. Geophys. Res.*, doi:10.1002/2013JD019912.

Colarco, P., M. Schoeberl, B. Doddridge, L. Marufu, O. Torres, and E. Welton. (2004) Transport of smoke from Canadian forest fires to the surface near Washington, D.C.: Injection height, entrainment, and optical properties, *J. Geophys. Res.*, 109, D06203, doi:10.1029/2003jd00424.

Couwenberg, J., R. Dommain, and H. Joosten, H. (2010). Greenhouse gas fluxes from tropical peatlands in south-east Asia. Global Change Biology, 16: 1715–1732. doi:10.1111/j.1365-2486.2009.02016.

Delene, D. J. and J.A. Ogren (2002) Variability of aerosol optical properties at four North American surface monitoring sites, J. Atmos. Sci., 59(6), 1135–1150.

Dennis, R. A., J. Mayer, G. Applegate, U. Chokkalingam, C.J.P. Colfer, I. Kurniawan, and T.P. Tomich. (2005). Fire, people and pixels: linking social science and remote sensing to understand underlying causes and impacts of fires in Indonesia. *Human Ecology*, *33*(4), 465-504.

Dubovik, O., A. Smirnov, B.N. Holben, M.D. King, Y.J. Kaufman, T.F. Eck and I Slutsker. (2000) Accuracy assessments of aerosol optical properties retrieved from Aerosol Robotic Network (AERONET) Sun and sky radiance measurements. J. Geophys. Res., 105(D8), 9791-9806.

Ekman, A., A. Engstrom and C. Wang. (2007). The effect of aerosol composition and concentration on the development and anvil properties of a continental deep convective cloud, Q. J. Roy. Meteor. Soc., 133B(627), 1439-1452.

Ekman, A. M. L., M. Hermann, P. Gross, J. Heintzenberg, D. Kim, and C. Wang. (2012). Sub-micrometer aerosol particles in the upper troposphere/lowermost stratosphere as measured by CARIBIC and modeled using the MIT-CAM3 global climate model, *J. Geophys. Res*., 117, D11202, doi:10.1029/2011JD016777.

Field, R. D., G.R. van der Werf, S.P.P. Shen. (2009) Human amplification of drought-induced biomass burning in Indonesia since 1960. *Nature Geosci.*, 10.1038/ngeo443.

Freeborn, P. H., M.J. Wooster, D.P. Roy and M.A. Cochrane. (2014). Quantification of MODIS fire radiative power (FRP) measurement uncertainty for use in satellite-based active fire characterization and biomass burning estimation, *Geophys. Res. Lett.*, 41, 1988–1994, doi:10.1002/2013GL59086.

Giglio, L., I. Csiszar and C.O. Justice. (2006) Global distribution and seasonality of active fires as observed with the Terra and Aqua MODIS sensors. *J. Geophys. Res.*, doi:10.1029/2005JG000142.

Hansen, M. C. (2008). Humid tropical forest clearing from 2000 to 2005 quantified by using multitemporal and multiresolution remotely sensed data. Proc. Natl. Acad. Sci. USA, 105, 9439–9444.

Hostetler, C., Hair, J., Liu, Z.Y., Ferrare, R., Harper, D., Cook, A., Vaughan, M., Trepte, C., Winker. D. (2008) Validation of CALIPSO Lidar Observations Using Data From the NASA Langley Airborne High Spectral Resolution Lidar (Retrieved from: https://ntrs.nasa.gov/archive/nasa/casi.ntrs.nasa.gov/20080014234.pdf)

Hostetler, C, Z. Liu, J. Reagan, M. Vaughan, D. Winker, M. Osborn, W. Hunt, K. Powell, and C. Trepte. (2006). CALIOP Algorithm Theoretical Basis Document–Part 1: Calibration and Level 1 Data Products. *Doc. PC-SCI* 201.

Ichoku, C., L. Giglio, M. Wooster and L. Remer. (2008). Global characterization of biomass-burning

patterns using satellite measurements of fire radiative energy. *Remote Sensing of Environment* 112.6, 2950-2962.

Kahn, R.A., Chen, Y., Nelson, D.L., Leung, F.Y., Li, Q.B., Diner, D.J., and Logan, J.A. (2008). Wildfire smoke injection heights: Two perspectives from space. *Geophys. Res. Lett.*, 35, L04809, doi:10.1029/2007GL032165.

Kahn, R.A., Li, W.H., Moroney, C., Diner, D.J., Martonchik, J.V., and Fishbein, E. (2007). Aerosol source plume physical characteristics from space-based multiangle imaging. *J. Geophys. Res.*, 112, D11205, doi:10.1029/2006JD007647, 2007

Kalnay et al. (1996). The NCEP/NCAR 40-year reanalysis project, Bull. Amer. Meteor. Soc., 77, 437-470.

Kaufman, Y. J., C. Ichoku, L. Giglio, S. Korontzi, D.A. Chu, W.M. Hao, and C.O. Justice. (2003). Fire and smoke observed from the Earth Observing System MODIS instrument--products, validation, and operational use. *International Journal of Remote Sensing*, *24*(8), 1765-1781.

Kim, D., C. Wang, A.M.L. Ekman, M. C. Barth, and P. Rasch. (2008) Distribution and direct radiative forcing of carbonaceous and sulfate aerosols in an interactive size-resolving aerosol-climate model, *J. Geophys. Res*., 113, D16309, doi:10.1029/2007JD009756.

Lamarque, J. F. (2010). Historical (1850–2000) gridded anthropogenic and biomass burning emissions of reactive gases and aerosols: methodology and application. *Atmos. Chem. Phys.*, doi:10.5194/acp-10-7017-2010.

Langmann, B., B. Duncan, C. Textor, J. Trentmann, and G.R. van der Werf. (2009). Vegetation fire emissions and their impact on air pollution and climate. *Atmospheric Environment*, *43*(1), 107-116.

Lee, J., Hsu, N.C., Bettenhausen, C., Sayer, A.M., Seftor, C.J., Jeong, M.J., Tsay, S.C., Welton, E.J., Wang, S.H., Chen, W.N. (2016) Evaluating the Height of Biomass Burning Smoke Aerosols Retrieved from Synergistic Use of Multiple Satellite Sensors over Southeast Asia, Aerosol and Air Quality Research, 16: 2831–2842 doi:10.4209/aaqr.2015.08.0506

Leung, F.Y.T., J.A. Logan, R. Park, E. Hyer, E. Kasischke, D. Streets, and L. Yurganov. (2007) Impacts of enhanced biomass burning in the boreal forests in 1998 on tropospheric chemistry and the sensitivity of model results to the injection height to emissions. *J. Geophys. Res.*, 112, D10313, doi:10.1029/2006JD008132.

Lin, N. H., A.M. Sayer, S.H. Wang, A.M. Loftus, T.C. Hsiao, G.R. Sheu, and S. Chantara. (2014). Interactions between biomass-burning aerosols and clouds over Southeast Asia: Current status, challenges, and perspectives. *Environmental Pollution*, *195*, 292-307.

Martin, V.M., R.A. Kahn, J.A. Logan, R. Paugam, M. Wooster, and C. Ichoku. (2012). Space-based observational constraints for 1-D fire smoke plume-rise models. *Journal of Geophysical Research: Atmospheres (1984–2012)*, *117*(D22).

Miettinen, J., E. Hyer, A.S. Chia, L.K. Kwoh, and S.C. Liew, S. C. (2013). Detection of vegetation fires and burnt areas by remote sensing in insular Southeast Asian conditions: current status of knowledge and future challenges. *International journal of remote sensing*, *34*(12), 4344-4366.

516 Ming, Y., V. Ramaswamy and G. Persad. (2010) Two opposing effects of absorbing aerosols on global-
517 mean precipitation. *Geophysical Research Letters* 37.13.
518 Nakajima, T., A. Higurashi, N. Takeuchi and J.R. Herman (1999). Satellite and ground-based study of
519 optical properties of 1997 Indonesian Forest Fire aerosols. Geophys. Res. Lett.,
520 10.1029/1999GL900208.
521 Petersen, W. and S. Rutledge. (2001). Regional Variability in Tropical Convection: Observations from
522 TRMM. J. Climate, 14, 3566–3586.
523 Petrenko, M., R.A. Kahn, M. Chin, A.J. Soja, T. Kucsera, and Harshvardhan. (2012) The use of satellite-
524 measured aerosol optical depth to constrain biomass burning emissions source strength in the global
525 model GOCART, *J. Geophys. Res.*, doi:10.1029/2012JD01787.
526 Rienecker, M.M., M.J. Suarez, R. Gelaro, R. Todling, J. Bacmeister, E. Liu, M.G. Bosilovich, S.D.
527 Schubert, L. Takacs, G.-K. Kim, S. Bloom, J. Chen, D. Collins, A. Conaty, and A. da Silva (2011).
528 MERRA: NASA's Modern-Era Retrospective Analysis for Research and Applications. J. Climate,
529 24, 3624-3648, doi:10.1175/JCLI-D-11-00015.1
530 Rogers, R.R., Hostetler, C.A., Ferrare, R.A., Hair, J.W., Obland, M.D., Cook, A.L., Harper, D.B., Swanson,
531 A.J. (2009) Validation of CALIOP Aerosol Backscatter and Extinction Profile Products Using
532 Airborne High Spectral Resolution Lidar Data (Retrieved from:
533 http://cimss.ssec.wisc.edu/calipso/meetings/cloudsat_calipso_2009/Posters/Rogers.pdf)
534 Schuster, G. L., O. Dubovik, B. Holben and E. Clothiaux. (2005) Inferring black carbon content and
535 specific absorption from Aerosol Robotic Network (AERONET) aerosol retrievals, *J. Geophys.*
536 *Res.*, 110, D10S17, doi:10.1029/2004JD004548.
537 Sessions, W. R., H.E. Fuelberg, R.A. Kahn, and D.M. Winker. (2011). An investigation of methods for
538 injecting emissions from boreal wildfires using WRF-Chem during ARCTAS. *Atmospheric*
539 *Chemistry and Physics*, *11*(12), 5719-5744.
540 Sofiev, M., T. Ermakova, and R. Vankevich. (2012). Evaluation of the smoke-injection height from
541 wildland fires using remote-sensing data. *Atmos. Chem. Phys*, vol. 12, no. 4, pp. 1995–2006.
542 Stone, P. and J. Carlson. (1979). Atmospheric Lapse Rate Regimes and Their Parameterization. J. Atmos.
543 Sci., 36, 415–423.
544 Sugimoto, N., Nishizawa T., Shimizu A., Matsui I., Jin Y. (2014) Characterization of aerosols in East Asia
545 with the Asian dust and aerosol lidar observation network (AD-Net) Proc. SPIE 9262 92620K
546 Sugimoto, N., Shimizu, A., Nishizawa, T., Matsui, I., Jin, Y., Khatri, P., Irie, H., Takamura, T., Aoki, K.,
547 Thana, B. (2014) Aerosol characteristics in Phimai, Thailand determined by continuous observation
548 with a polarization sensitive Mie–Raman lidar and a sky radiometer, Environmental Research
549 Letters, 10, 6.
550 Tao, W.K., J.P. Chen, Z.Q. Li, C. Wang, and C.D. Zhang. (2012) The Impact of Aerosol on convective
551 cloud and precipitation. *Rev. Geophys*., 50, RG2001, doi:10.1029/2011RG000369.
552 Taylor, D. (2010). Biomass burning, humans and climate change in Southeast Asia. *Biodiversity and*

conservation, *19*(4), 1025-1042.

Tosca, M. G., J.T. Randerson, C.S. Zender, D.L. Nelson, D.J. Diner, and J.A. Logan (2011), Dynamics of fire plumes and smoke clouds associated with peat and deforestation fires in Indonesia, *J. Geophys. Res*., 116, D08207, doi:10.1029/2010JD015148.

Tsigaridis, K., N. Daskalakis, M. Kanakidou, P.J. Adams, P. Artaxo, R. Bahadur, Y. Balkanski, S.E. Bauer, N. Bellouin, A. Benedetti, T. Bergman, T.K. Berntsen, J.P. Beukes, H. Bian, K.S. Carslaw, K. S., M. Chin, G. Curci, T. Diehl, R.C. Easter, S.J. Ghan, S.L., Gong, A. Hodzic, C.R. Hoyle, T. Iversen, S. Jathar, J.L. Jimenez, J.W. Kaiser, A. Kirkevag, D. Koch, H. Kokkola, Y.H. Lee, G. Lin, X. Liu, C. Luo, X. Ma, G.W. Mann, N. Mihalopoulos, J.J. Morcrette, J.F. Müller, G. Myhre, S. Myriokefalitakis, N.L. Ng, D. O'Donnell, J.E. Penner, L. Pozzoli, K.J. Pringle, L.M. Russell, M. Schulz, J. Sciare, O. Seland, D.T. Shindell, S. Sillman, R.B. Skeie, D. Spracklen, T. Stavrakou, S.D. Steenrod, T. Takemura, P. Tiitta, S. Tilmes, H. Tost, T. van Noije, P.G. van Zyl, K. von Salzen, F. Yu, Z. Wang, Z. Wang, R.A. Zaveri, H. Zhang, K. Zhang, Q. Zhang, and X. Zhang, X. (2014) The AeroCom evaluation and intercomparison of organic aerosol in global models, Atmos. Chem. Phys., 14, 10845-10895, doi:10.5194/acp-14-10845-2014.

van der Werf, G. R. (2010). Global fire emissions and the contribution of deforestation, savanna, forest, agricultural, and peat fires (1997–2009). *Atmos. Chem. Phys.*, 10.5194/acp-10-11707-2010.

van der Werf, G. R., J. Dempewolf, S.N. Trigg, J.T. Randerson, P.S. Kasibhatla, L. Giglio, and R.S DeFries. (2008). Climate regulation of fire emissions and deforestation in equatorial Asia. *Proceedings of the National Academy of Sciences*, *105*(51), 20350-20355.

Wang, C. (2013) Impact of anthropogenic absorbing aerosols on clouds and precipitation: A review of recent progresses, *Atmos. Res*., 122, 237-249.

Wang, C. (2007). Impact of direct radiative forcing of black carbon aerosols on tropical convective precipitation, Geophys. Res. Lett., 34, L05709, doi:10.1029/2006GL028416.

Winker, D. M., J. Pelon, and M.P. McCormick (2003), The CALIPSO mission: Spaceborne lidar for observation of aerosols and clouds, *Proc. SPIE*, **4893**, 1–11.

Woodward J. L. (2010). *Estimating the Flammable Mass of a Vapour Cloud: A CCPS Concept Book*, John Wiley & Sons, ISBN 0470935359, 9780470935354.

Wooster, M. J., G.L.W. Perry and A. Zoumas. (2012) Fire, drought and El Niño relationships on Borneo (Southeast Asia) in the pre-MODIS era (1980–2000), Biogeosciences, 9, 317-340, doi:10.5194/bg-9-317-2012.

584 **Table 1**: Statistical summary of measured (CALIPSO) smoke plume heights in October 2006, at different
585 percentiles of extinction height (top/Z=10%, middle-upper/ Z=30%, median/Z=50%, middle-lower/Z=70%,
586 and bottom/Z=90%), over the subset of the Maritime Continent **impacted by smoke** (**FIRE**), and **not**
587 **impacted by smoke** (**NO-FIRE**), based on MISR observations (**Figure 1).** "MEAN" is average, "STD" is
588 standard deviation, and percentages XX% are the corresponding distribution's percentiles. Days which are
589 statistical outliers (mean >**85%** or <**15%** of at least one variable) are listed as **1st**, **3rd**, etc.

	bottom [km]	middle-lower [km]	median [km]	middle-upper [km]	top [km]
FIRE 5%	0.18	0.36	0.56	0.89	1.31
FIRE 10%	0.25	0.49	0.76	1.09	1.53
FIRE 15%	0.31	0.59	0.92	1.29	1.67
FIRE 50%	1.38	1.59	1.83	2.22	2.82
FIRE 85%	2.75	2.92	3.13	3.37	3.70
FIRE 90%	3.14	3.30	3.45	3.72	4.07
FIRE 95%	4.18	4.38	4.70	5.56	5.65
FIRE MEAN	1.68	1.92	2.17	2.50	2.98
FIRE STD	1.59	1.55	1.53	1.54	1.55
NO-FIRE 5%	0.16	0.33	0.48	0.60	0.70
NO-FIRE 10%	0.19	0.38	0.55	0.68	0.87
NO-FIRE 15%	0.21	0.42	0.59	0.77	1.12
NO-FIRE 50%	0.31	0.57	0.83	1.25	1.76
NO-FIRE 85%	1.16	1.64	2.01	2.36	2.85
NO-FIRE 90%	1.65	1.98	2.27	2.60	3.05
NO-FIRE 95%	2.22	2.45	2.73	2.99	3.41
NO-FIRE MEAN	0.97	0.98	1.00	1.02	1.08
NO-FIRE STD	0.65	0.93	1.21	1.53	1.98

590

591 **Table 2**: Summary of measured (CALIPSO) smoke plume heights in October 2006, for days that are
592 statistical outliers **mean (>85% or <15%) of all data in bold**, mean (>80% or <20%) of all data in regular
593 text. The levels are given as a percentile of extinction height over the subset of the Maritime Continent
594 **impacted by smoke** (fire-constrained), based on MISR observations (**Figure 1).**

	bottom (90% Extinction) [km]	middle-lower (70% Extinction) [km]	median (50% Extinction) [km]	middle-upper (30% Extinction) [km]	top (10% Extinction) [km]
FIRE 11th	2.29	2.54	**3.26**	**4.11**	**4.93**
FIRE 15th	1.85	2.20			
FIRE 22nd	**2.55**	**2.85**	2.95		

595

596 **Table 3**: Monthly statistics of measured fire properties (FRP and T_F), for all measured fires (**ALL**) and
597 level 9 confidence fires (**L9**) and MERRA meteorological properties (T_A, v, U, dT/dz) corresponding to the
598 geographic locations of **L9**. All data is constrained by the boundaries of the fire extent in October 2006
599 (**Figure 1**). The distribution's percentile is given as "**XX%**", the mean and standard deviation are given as
600 "**MEAN**" and "**STD**". Note that there were no observed fires of L9 on the following dates: 17th, 22nd, 23rd,
601 24th, 25th, 26th, 27th, 29th, 31st.

	FRP **ALL** [W/m^2]	FRP **L9** [W/m^2]	T_F **ALL** [K]	T_F **L9** [K]	T_A **L9** [K]	V **L9** [mm/s]	U **L9** [m/s]	dT/dz **L9** [K/km]
5%	95.	140.	370.	410.	296.0	0.2	4.1	-5.25
10%	115.	185.	390.	445.	296.4	0.4	4.4	-5.27
15%	130.	230.	400.	480.	296.6	0.6	4.5	-5.28
50%	300.	540.	535.	725.	298.4	1.5	6.0	-5.43
85%	775.	1240.	910.	1275.	301.1	4.1	7.4	-5.65
90%	975.	1495.	1070.	1525.	301.5	4.6	7.7	-5.69
95%	1290.	1855.	1335.	1850.	302.1	5.6	8.1	-5.75
Mean	510.	920.	702.	1029.	298.7	2.1	6.0	-5.44
StD	720.	1340.	573.	1057.	2.0	1.6	1.3	0.16

602

603 **Table 4**: Monthly statistics of modeled aerosol heights, based upon level 9 confidence fires (**L9**) and
604 MERRA meteorological properties (T_A, v, U, dT/dz) at the corresponding geographic locations. Sensitivity
605 tests are shown with their respective weighting factor (**1.2, 1.4, 1.6, 1.8, or 2.0**) applied to the measured
606 FRP. The modeled heights are given by percentile from the bottom (5%) to the top (95%), while the mean
607 and standard deviation are given as "**MEAN**" and "**STD**". Note that the model was not run on the
608 following days, during which there were no observed **L9** fires: 17th, 22nd, 23rd, 24th, 25th, 26th, 27th, 29th, and
609 31st.

	FRP(x1.0) [km]	**FRP(x1.2) [km]**	**FRP(x1.4) [km]**	**FRP(x1.6) [km]**	**FRP(x1.8) [km]**	**FRP(x2)[km]**
5%	**0.41**	0.44	0.48	0.53	0.56	0.60
10%	**0.60**	0.67	0.73	0.80	0.85	0.91
15%	**0.75**	0.83	0.91	0.98	1.05	1.12
30%	**1.14**	1.28	1.40	1.52	1.63	1.74
50%	**1.85**	2.07	2.27	2.47	2.65	2.82
70%	**2.87**	3.23	3.54	3.84	4.12	4.38
85%	**4.21**	4.66	5.11	5.53	5.87	6.22
90%	**4.99**	5.54	6.08	6.58	6.97	7.41
95%	**6.10**	6.79	7.43	7.76	8.16	8.61
Mean	**2.41**	2.69	2.96	3.21	3.44	3.67
StD	**1.98**	2.21	2.42	2.62	2.81	2.99

610

Figure 1: Map of Maritime Continent. The smoke plume impacts the sub-region contained within the dashed lines, or the so-called **fire-constrained** region. On the other hand, the region outside of the dashed lines is the so-called **non fire-constrained** region. The plot is based on a variance maximization technique applied to the measurements from all MISR overpasses from 2000 through 2014 (*Cohen*, 2014). Note that in this part of the world 1 degree of latitude or longitude is approximately 100km, leading to a fire-impacted region over 2500km across.

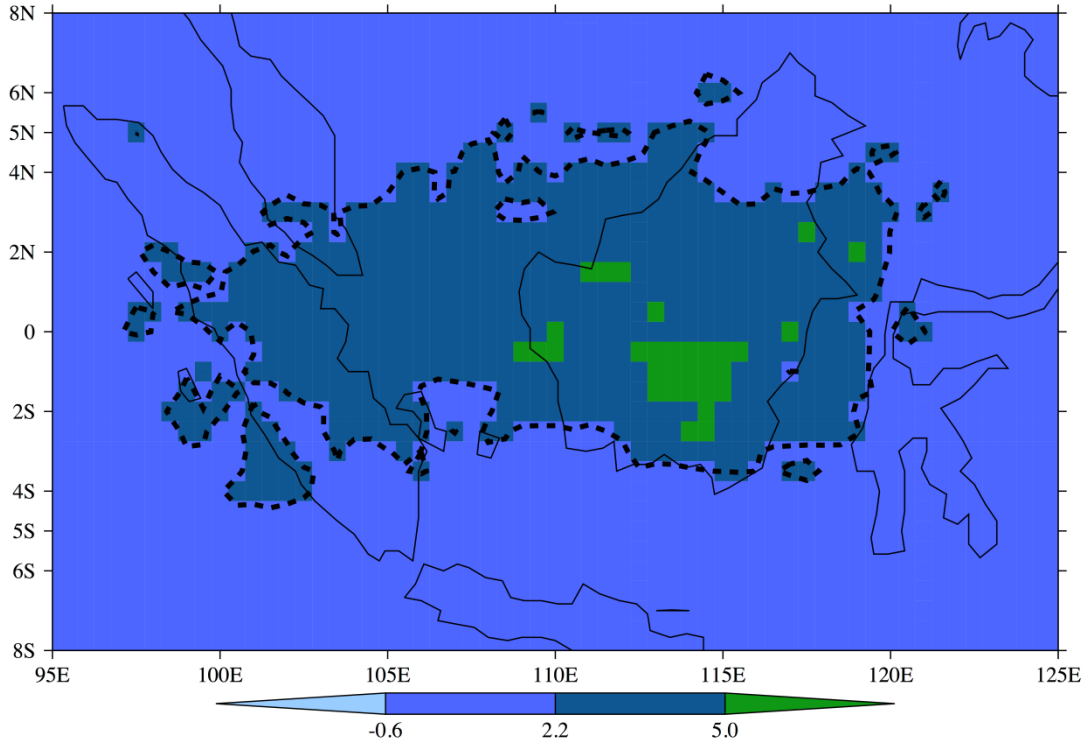

Figure 2a,2b: Time series of measured CALIPSO extinction heights over the fire constrained (A) and non fire-constrained (B) regions as given **Figure 1**. For both plots, the dots correspond to the height of the column integrated backscatter at: 10% [red] (top), 30% [dark blue], 50% [yellow], 70% [black], and 90% [light blue] (bottom). The circles are computed daily means, while dots are the computed daily standard deviation bands. There was no measurement over the region on the 10th, 16th, and 20th.

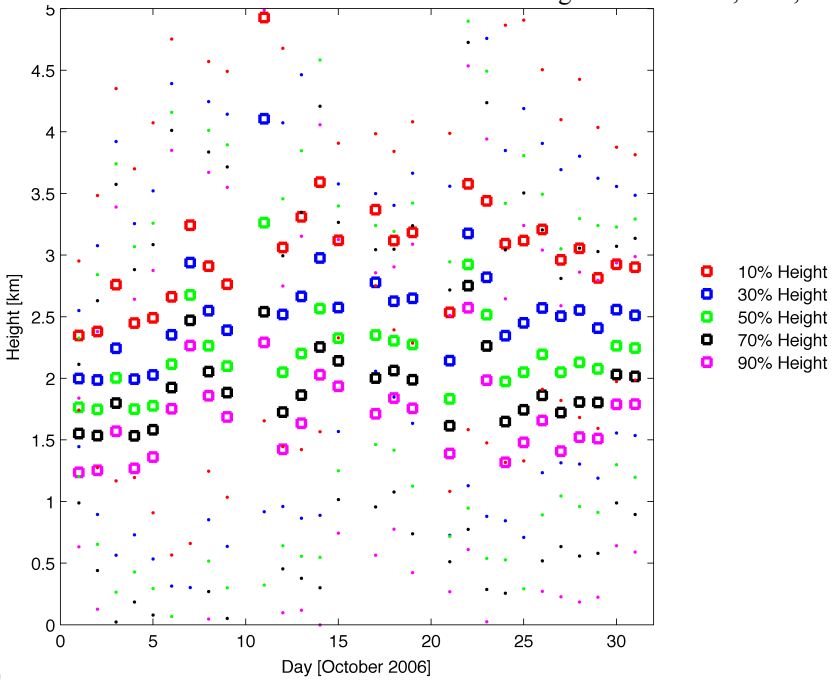

(A)

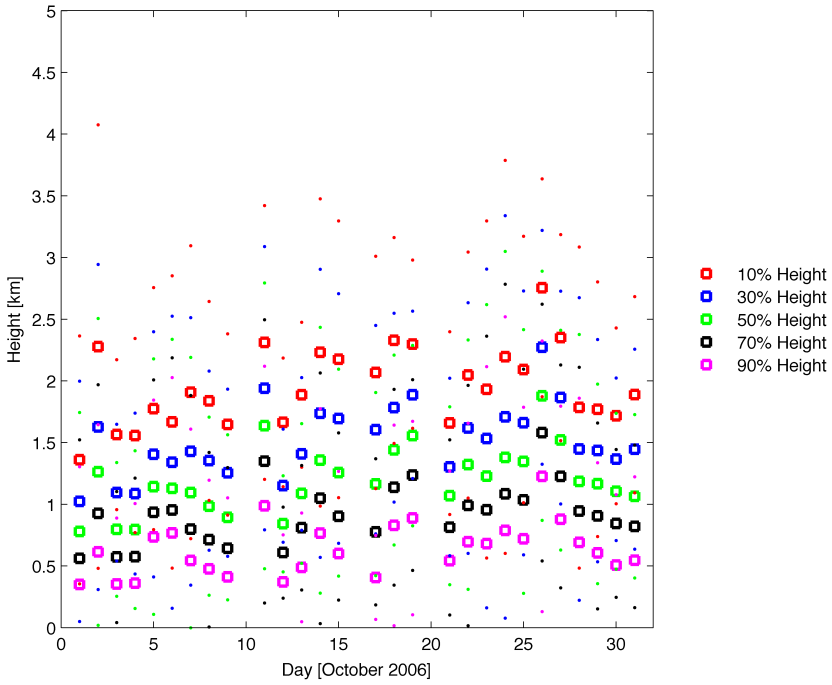

(B)

Figure 3: Time series of daily averaged measured AOD over the fire-constrained regions of the Maritime Continent [blue], and the non fire-constrained regions of the Maritime Continent [red], as given in **Figure 1**. Circles are computed daily mean values, while dots are computed daily standard deviation bands.

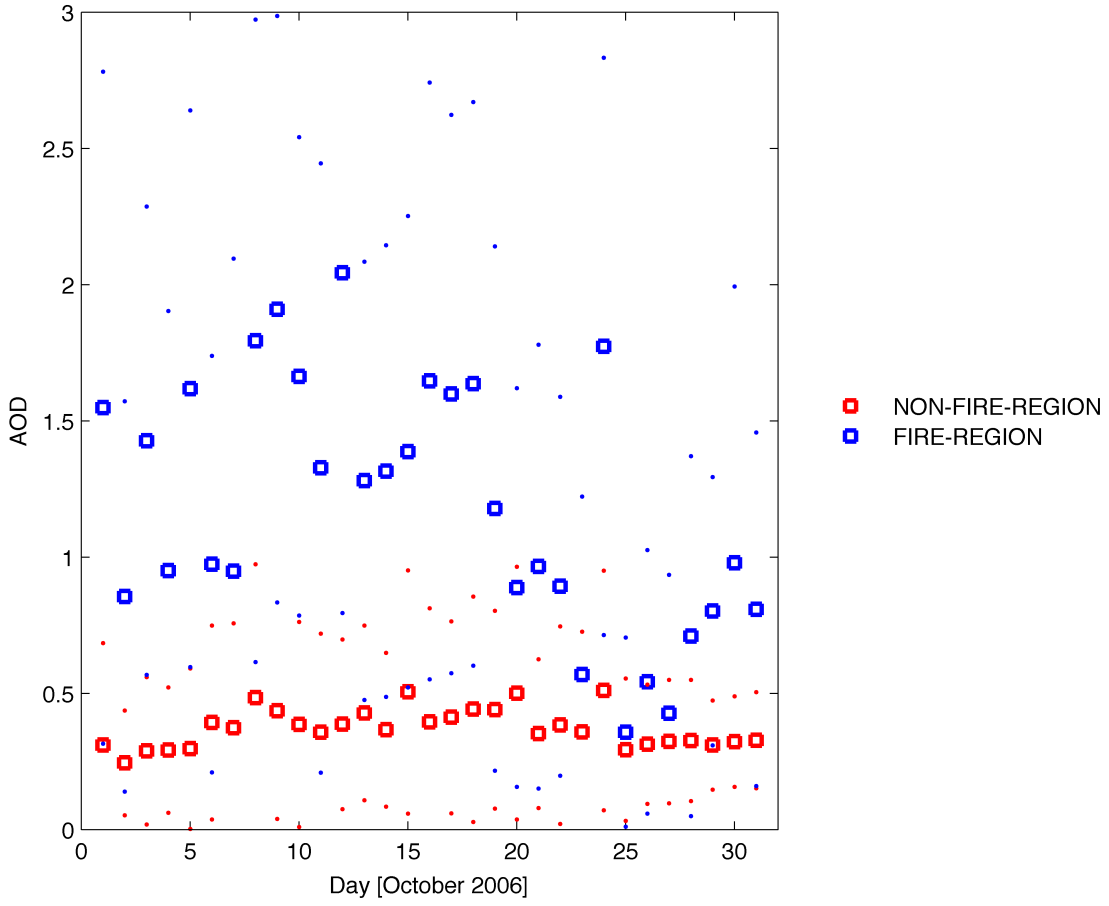

Figure 4: Time series of PDFs (20% and 80% values are stars and mean values are given by lines) of the measured extinction heights for middle-upper (blue), median (red), and middle-lower (green) levels. The best fitting modeled heights are given as 0% FRP enhancement (solid black line) (best fit for middle-upper measurements), 20% FRP enhancement (dashed black line) (best fit for median measurements), and 100% FRP enhancement (dotted black line) (best fit for the middle-lower measurements).